Earthline Journal of Mathematical Sciences
E-ISSN: 2581-8147
Volume 15, Number 1, 2025, Pages 35-58
https://doi.org/10.34198/ejms.15125.035058

Chemical Reaction and Cross Diffusion Effects on Heat and Mass Transfer Characteristics of Viscoelastic Oil-Based Nanofluid Over a Porous Nonlinear Stretching Surface

Christian John Etwire[1,*], Ibrahim Yakubu Seini[2], Rabiu Musah[3] and Oluwole Daniel Makinde[4]

[1] Department of Mathematics, School of Mathematical Sciences, C. K. Tedam University of Technology and Applied Sciences, P.O. Box 24, Navrongo, Ghana
e-mail: jecpapa@yahoo.com

[2] Department of Mechanical & Industrial Engineering, School of Engineering, University for Development Studies, Nyankpala Campus, P.O. Box 1882, Tamale, Ghana
e-mail: dr.yseini@uds.edu.gh

[3] Department of Physics, School of Engineering, University for Development Studies, Nyankpala Campus, P.O. Box 1882, Tamale, Ghana
e-mail: mrabiu@uds.edu.gh

[4] Faculty of Military Science, Stellenbosch University, Private Bag X2, Saldanha 7395, South Africa
e-mail: makinded@gmail.com

Abstract

The impact of chemical reaction and cross diffusion on heat and mass transport characteristics of viscoelastic flow of Al_2O_3 and CuO oil-based nanofluids past a porous nonlinear stretching surface has been examined. Similarity transformation was used to transform the governing partial differential equations into coupled nonlinear ordinary differential equations and solved numerically by employing the fourth order Runge-Kutta algorithm with a shooting method. Results for the entrenched parameters controlling the flow dynamics have been tabulated and illustrated graphically. The results found CuO-oil based nanofluid to exhibit higher mass transfer rate and lower heat transfer rate and skin friction coefficient than Al_2O_3-oil based nanofluid under the same viscoelastic condition. This indicates that CuO-oil based nanofluid can be used as the working fluid in mechanical dampers.

Nomenclature

(x, y) = Cartesian coordinates	h_f = Heat transfer coefficient
(u, v) = Velocity components along x and y axes	Pr = Prandtl number
T_f = Temperature of hot fluid	C_f = skin-friction coefficient
T_∞ = Free-stream temperature of nanofluid	Re = Reynolds number
T_w = Temperature of the sheet	Nu = Nusselt number
T = Temperature of nanofluid	q_w = Wall heat flux
k_f = Thermal conductivity of oil	Br = Brinkman number
k_s = Thermal conductivity of nanoparticles	U_∞ = Free stream velocity of nanofluid
c_p = Specific heat at constant pressure	S = Suction parameter

Received: February 25, 2023; Revised: November 3, 2024; Accepted: November 13, 2024; Published: November 27, 2024
2020 Mathematics Subject Classification: 76-10, 76A05, 76D05.
Keywords and phrases: Dufour effect, Soret effect, viscoelastic flow, nonlinear stretching, diffusion.
*Corresponding author

k' = Permeability of the porous media	C = Concentration of nanofluid
K^* = Permeability parameter	C_∞ = Free-stream concentration of nanofluid
D_m = Mean diffusion coefficient	C_w = Concentration of the sheet
k_t = Thermal-diffusion ratio	D_B = Brownian diffusion coefficient
c_s = Concentration susceptibility of the nanofluid	T_m = Mean temperature of the nanofluid
Bi = Biot number	Sc = Schmidt number
S_o = Soret number	Sh = Sherwood number

Symbols

η = Dimensionless Variable	φ = Solid volume fraction of nanoparticles
τ_w = Wall shear stress	$(\rho c_p)_{nf}$ = Heat capacitance of nanofluid
μ_{nf} = Dynamic viscosity of nanofluid	ψ = Stream function
υ_f = Kinematic viscosity of oil	θ = Dimensionless Temperature
ρ_{nf} = Density of nanofluid	γ = Reaction rate parameter
α = Thermal diffusivity of oil	$\phi(\eta)$ = Dimensionless concentration
ρ_f = Density of oil	α_v = Viscoelastic parameter
ρ_s = Density of nanoparticles	β = Chemical reaction rate parameter

1. Introduction

Many engineering designs and industrial processes involve simultaneous heat and mass transfers. This phenomenon gives rise to cross-diffusion effect. Thermal diffusion effect (Soret effect) arises as a result of mass transfer by temperature gradient while Diffusion-thermo effect (Dufour effect) is due to the heat transfer by concentration gradient. Cross diffusion effects occur in processes such as materials' processing and exploiting, fabrication of semiconductor devices in molten metal and oil recovery from hydrocarbon reservoirs. Due to these applications, research on the influence of thermal diffusion and diffusion-thermo effects on flow dynamics are gaining interest from researchers and scientists. Awad *et al.* [1] examined thermo diffusion effects on magneto-nanofluid flow over a stretching sheet. While Hayat *et al.* [2] analyzed Soret and Dufour effects on MHD peristaltic flow of Jeffrey fluid in a rotating system with porous medium. Kasmani *et al.* [3] presented exciting results on convection flow of nanofluid past a moving wedge with Soret and Dufour effects. Salleh *et al.* [4] examined Dufour and Soret effects on MHD boundary layer slips flow in nanofluids with microorganisms over a heated stretching sheet with temperature-dependent viscosity. Rao *et al.* [5] explored Soret and Dufour effects on magneto-nanofluid flow over a stretching sheet in the presence of thermal radiation and heat generation/absorption. Najib *et al.* [6] discussed the stability of stagnation-point flow in a nanofluid over a stretching/shrinking sheet with second-order slip, Soret and Dufour effects. Kumar *et al.* [7] studied cross diffusion effects on heat and mass transfer micropolar fluid flow past a stretching surface. Sharma *et al.* [8] reported on Soret and Dufour effects on viscoelastic radiative and heat absorbing nanofluid driven by a stretched sheet with inclined magnetic field. Kandasamy *et al.* [9] elucidated the effects of thermal and solutal stratification on MHD nanofluid flow over a porous vertical plate. The influence of nonlinear radiation and cross diffusion on magnetohydrodynamic flow of Casson and Walters-B nanofluids past a variable thickness sheet was investigated by Lakshmi *et al.* [10]. Bhuvaneswari *et al.* [11] evaluated the effects of cross-diffusion on MHD mixed convection over a stretching surface in a porous medium with chemical reaction and convective condition. Aghbari *et al.* [12] reported on the Soret and Dufour effect on non-Darcy natural convection flow of Buongiorno nanofluid over a vertical plate in a porous medium with viscous dissipation. Idowu and Falodun

[13] examined Soret-Dufour effects on MHD heat and mass transfer of Walter's-B viscoelastic fluid over a semi-infinite vertical plate. Bhaskar *et al*. [14] employed optimal homotopy technique to study the effects of cross diffusion on MHD fluid flow through a channel. Baako *et al*. [15] explored the impact of Dual Stratification on mixed convective Electro-magnetohydrodynamic flow over a stretching plate with multiple slips and cross diffusion. Chitra *et al*. [16] investigated the effects of cross diffusion on radiative MHD flow over a rotating cone through porous medium. Kumar *et al*. [17] analyzed the effects of cross diffusion on radiative MHD flow over a rotating cone through porous medium.

Many industrial processes involve fluids such as paint, crude oil, asphalt, polymers and grease which are viscoelastic. At very low temperature, they solidify while at very high temperature, their shearing stresses are proportional to their rate of shearing strains. These fluids find applications in the manufacturing, petroleum, chemical and automobile industries. For instance, lubricating grease is used in automotive to absorb noise, vibration and harshness as well as in a journal bearing for sealing, anti-friction and wear and tear reduction. Due to these applications, research on heat and mass transport potential of viscoelastic fluids is gaining interest. Sahoo and Biswal [18] provided interesting results for MHD viscoelastic boundary layer flow past a stretching plate with heat transfer. Shit *et al.* [19] discussed convective heat transfer and MHD viscoelastic nanofluid flow induced by a stretching sheet. The effect of viscoelastic oil-based nanofluids on a porous nonlinear stretching surface with variable heat source/sink was reported by Etwire *et al.* [20]. Narayana *et al.* [21] studied MHD stagnation point flow of viscoelastic nanofluid past a convectively heated stretching surface. Mahat *et al.* [22] analyzed mixed convection boundary layer flow of viscoelastic nanofluid past a horizontal circular cylinder with convective boundary condition. Hussain *et al.* [23] proposed a model for MHD viscoelastic nanofluid flow with radiation effects. Chaich *et al.* [24] thermodynamically analyzed viscoelastic fluid flow in a porous medium with prescribed wall heat flux over stretching sheet subjected to a transitive magnetic field. Aloliga *et al*. [25] explored MHD flow of Non-Newtonian viscoelastic fluid over a stretched magnetized surface. Nan *et al.* [26] numerically studied radiative MHD flow of viscoelastic fluids with distributed-order and variable-order space fractional operators.

It is evident from the survey of literature that the study on the transport dynamics of viscoelastic flow of oil-based nanofluid with cross diffusion effects has not been tackled. Hence, this study seeks to examine the impact of chemical reaction and cross diffusion on heat and mass transport characteristics of viscoelastic flow of oil-based nanofluids past a porous nonlinear stretching surface. The rest of the paper is organized as follows: The mathematical model is presented in Section 2 while similarity transformation in Section 3. The Computational Method is outlined in Section 4 with results and discussions presented in Section 5. Section 6 presents the Conclusion.

2. Mathematical Model

Consider a heat and mass transfer of two-dimensional steady incompressible flow of dielectric and chemically reacting viscoelastic oil-based nanofluid containing Al_2O_3 and CuO over a porous nonlinear stretching plate with thermal diffusion and diffusion-thermo effects. The x-axis is taken along the direction of the porous nonlinear stretching plate whilst the y-axis is taken normal to it as illustrated in Figure 1. The lower surface of the plate is heated by convection from a hot fluid at temperature T_f, which provides a heat transfer coefficient h_f while a stream of oil based nanofluid with free stream temperature T_∞ and concentration C_∞ moves over the right surface of the plate with a uniform free stream velocity U_∞. The velocity of the nonlinear stretching surface is assumed to be proportional to the n^{th} power of the displacement *x,* from the origin (that is $U_w = bx^n$).

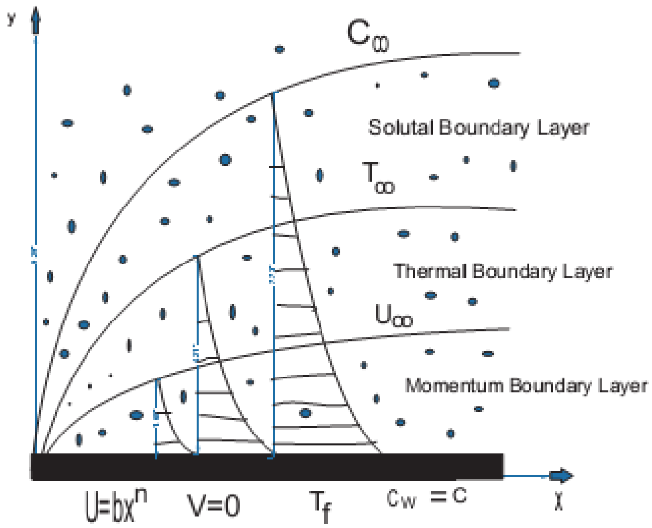

Figure 1: Schematic diagram of flow problem.

It is assumed that both the oil and nanoparticles are in thermal equilibrium with no slip between them. The variation of density in the nanofluid is taken into account using the Boussinesq approximation. The continuity, momentum, energy and concentration equations modeling the flow problem can be expressed as;

$$\frac{\partial u}{\partial x}+\frac{\partial v}{\partial y}=0, \tag{1}$$

$$u\frac{\partial u}{\partial x}+v\frac{\partial u}{\partial y}=\frac{\mu_{nf}}{\rho_{nf}}\frac{\partial^2 u}{\partial y^2}-\frac{\mu_{nf}}{\rho_{nf}k'}u-\frac{k_0}{\rho_{nf}}\left(v\frac{\partial^3 u}{\partial y^3}+u\frac{\partial^3 u}{\partial x\partial y^2}+\frac{\partial u}{\partial x}\frac{\partial^2 u}{\partial y^2}-\frac{\partial u}{\partial y}\frac{\partial^2 u}{\partial x\partial y}\right), \tag{2}$$

$$u\frac{\partial T}{\partial x}+v\frac{\partial T}{\partial y}=\frac{k_{nf}}{(\rho c_p)_{nf}}\frac{\partial^2 T}{\partial y^2}+\frac{\mu_{nf}}{(\rho c_p)_{nf}}\left(\frac{\partial u}{\partial y}\right)^2+\frac{k_0}{(\rho c_p)_{nf}}\left(u\frac{\partial^2 u}{\partial x\partial y}\frac{\partial u}{\partial y}+v\frac{\partial^2 u}{\partial y^2}\frac{\partial u}{\partial y}\right)+\frac{D_m k_t}{c_s c_p}\frac{\partial^2 C}{\partial y^2}, \tag{3}$$

$$u\frac{\partial C}{\partial x}+v\frac{\partial C}{\partial y}=D_B\frac{\partial^2 C}{\partial y^2}-\gamma(C-C_\infty)+\frac{D_m k_t}{T_m}\frac{\partial^2 T}{\partial y^2} \tag{4}$$

where u and v are x and y components of velocities respectively, μ_{nf} is the dynamic viscosity of the nanofluid, k_{nf} is the thermal conductivity of the nanofluid, ρ_{nf} is the density of the nanofluid, k' is the permeability of the porous media, k_0 is the coefficient of viscoelasticity, T is the temperature of the nanofluid, $(\rho c_p)_{nf}$ is the heat capacitance of the nanofluid, C is the concentration of the nanofluid, γ is the reaction rate parameter, D_B is the Brownian diffusion coefficient, D_m is the mean diffusion coefficient, k_t is the thermal-diffusion ratio, c_s is the concentration susceptibility of the nanofluid, c_p is the specific heat at constant pressure and T_m is the mean temperature of the nanofluid.

The boundary conditions on the surface of the plate at $y=0$ are;

$$u(x,0)=bx^n,\ \ v(x,0)=-v_w,\ \ -k_f\frac{\partial T}{\partial y}(x,0)=h_f\left[T_f-T(x,0)\right],\ \ C=C_w. \tag{5}$$

The boundary conditions of the oil-based nanofluid at the far surface of the plate as $y\to\infty$ are;

$$u(x,\infty)\to 0,\ \ \frac{\partial u(x,\infty)}{\partial y}\to 0,\ \ T(x,\infty)\to T_\infty,\ \ C\to C_\infty. \tag{6}$$

The properties of the nanofluid with spherical sized nanoparticles are defined [27, 28] as

$$\rho_{nf}=(1-\varphi)\rho_f+\varphi\rho_s, \tag{7}$$

$$\mu_{nf} = \frac{\mu_f}{(1-\varphi)^{2.5}}, \tag{8}$$

$$\left(\rho c_p\right)_{nf} = (1-\varphi)\left(\rho c_p\right)_f + \varphi\left(\rho c_p\right)_s, \tag{9}$$

$$k_{nf} = \frac{(k_s+2k_f)-2\varphi(k_f-k_s)}{(k_s+2k_f)+\varphi(k_f-k_s)}k_f, \tag{10}$$

where ρ_f and ρ_s are the reference densities of oil and nanoparticles respectively, φ is the solid volume fraction of the nanoparticles, k_f and k_s are the thermal conductivities of the base fluid and nanoparticles respectively and c_p is the specific heat at constant pressure and $(\rho c_p)_s$ is the heat capacitance of the nanoparticles.

3. Similarity Transformations

The continuity equation (1) is satisfied automatically, by defining the stream function, $\psi(x, y)$ in the usual way as;

$$u = \frac{\partial\psi}{\partial y} \quad \text{and} \quad v = -\frac{\partial\psi}{\partial x}. \tag{11}$$

A similarity solution of the equations (1)-(6) is achieved by defining an independent dimensionless variable, η, a stream function, ψ, in terms of a dependent variable $f(\eta)$, a dimensionless temperature $\theta(\eta)$ and a dimensionless concentration $\phi(\eta)$ as;

$$\eta = y\sqrt{\frac{b(n+1)}{2v_f}}x^{\frac{n-1}{2}}, \quad \psi = \sqrt{\frac{2bv_f}{n+1}}x^{\frac{n+1}{2}}f(\eta), \quad \theta(\eta) = \frac{T-T_\infty}{T_f-T_\infty}, \quad \phi(\eta) = \frac{C-C_\infty}{C_w-C_\infty}. \tag{12}$$

Substituting the relevant terms into equations (1)-(6) yields the coupled nonlinear differential equations as;

$$\frac{\rho_f}{(1-\varphi)^{2.5}\left((1-\varphi)\rho_f+\varphi\rho_s\right)}f'''(\eta) - \frac{2}{n+1}\frac{\rho_f K^*}{(1-\varphi)^{2.5}\left((1-\varphi)\rho_f+\varphi\rho_s\right)}f'(\eta)$$
$$-\frac{2n}{n+1}\left(f'(\eta)\right)^2 + f(\eta)f''(\eta)$$
$$-\frac{\rho_f\alpha_v}{[(1-\varphi)\rho_f+\varphi\rho_s]}\left[(3n-1)f'(\eta)f'''(\eta) - \frac{(3n-1)}{2}\left(f''(\eta)\right)^2 - \frac{(n+1)}{2}f(\eta)f''''(\eta)\right] = 0, \tag{13}$$

$$\frac{(k_s+2k_f)-2\varphi(k_f-k_s)}{(k_s+2k_f)+\varphi(k_f-k_s)}\theta''(\eta) + \frac{(1-\varphi)\left(\rho c_p\right)_f+\varphi\left(\rho c_p\right)_s}{\left(\rho c_p\right)_f}Pr\, f(\eta)\theta'(\eta) + \frac{Br}{(1-\varphi)^{2.5}}\left(f''(\eta)\right)^2$$
$$+Br\alpha_v\left[\frac{(3n-1)}{2}f'(\eta)\left(f''(\eta)\right)^2 - \frac{(n+1)}{2}f(\eta)f''(\eta)f'''(\eta)\right]$$
$$+\frac{(1-\varphi)\left(\rho c_p\right)_f+\varphi\left(\rho c_p\right)_s}{\left(\rho c_p\right)_f}Pr\, D_o\,\phi''(\eta) = 0, \tag{14}$$

$$\phi''(\eta) - \frac{2}{n+1}Sc\beta\phi(\eta) + Scf(\eta)\phi'(\eta) + ScS_o\theta''(\eta) = 0. \tag{15}$$

Subject to the boundary conditions;

$$f'(0) = 1,\ f(0) = S,\ \theta'(0) = -Bi(1-\theta(0)),\ \ \phi(0) = 1, \tag{16}$$

$$f'(\infty) \to 0,\ f''(\infty) \to 0,\ \theta(\infty) \to 0,\ \ \phi(0) \to 0, \tag{17}$$

where the prime symbol denotes differentiation with respect to η, $K^* = \frac{\upsilon_f}{bx^{n-1}k'}$ is the permeability parameter, $\alpha_v = \frac{k_o bx^{n-1}}{\mu_f}$ is the viscoelastic parameter, $\frac{D_m k_t}{c_s c_p}\frac{(C_w - C_\infty)}{\upsilon_f(T_f - T_\infty)} = D_o$ is the Dufour number, $S = \frac{V_w}{\sqrt{\frac{b\upsilon_f(n+1)}{2}}x^{\frac{n-1}{2}}}$ is the suction parameter, $\frac{h_f}{k_f\sqrt{\frac{b(n+1)}{2\upsilon_f}}x^{\frac{n-1}{2}}} = Bi$ is the Biot number, $\frac{\upsilon_f}{\alpha_f} = Pr$ is the Prandtl number and $\frac{\mu_f b^2 x^{2n}}{k_f(T_f - T_\infty)} = Br$ is the Brinkman number, $\frac{\upsilon_f}{D_B} = Sc$ is the Schmidt number, $\frac{\gamma}{bx^{n-1}} = \beta$ is the chemical reaction rate parameter and $\frac{D_m k_t}{T_m}\frac{(T_f - T_\infty)}{\upsilon_f(C_w - C_\infty)} = S_o$ is the Soret number.

The local skin-friction coefficient (C_f), Nusselt number (Nu) and Sherwood number (Sh) are the main parameters of engineering applications considered in the study. They are respectively defined as;

$$C_f = \frac{\tau_w}{\rho_f u_w^2}, \quad Nu = \frac{xq_w}{k_f(T_w - T_\infty)}, \quad Sh = \frac{xq_m}{D_B(C_w - C_\infty)}, \tag{18}$$

where τ_w is the wall shear stress, q_w is the wall heat flux and q_m is the wall mass flux which are respectively defined by;

$$\tau_w = \left[\mu_{nf}\frac{\partial u}{\partial y} + \frac{k_0}{\rho_{nf}}\left(u\frac{\partial^2 u}{\partial x \partial y} + v\frac{\partial^2 u}{\partial y^2} - 2\frac{\partial u}{\partial y}\frac{\partial v}{\partial y}\right)\right]_{y=0}, \quad q_w = -k_{nf}\frac{\partial T}{\partial y}\bigg|_{y=0}, \quad q_m = -D_B\frac{\partial C}{\partial y}\bigg|_{y=0}. \tag{19}$$

Substituting equation (19) into equation (18) yields;

$$C_f = \sqrt{\frac{n+1}{2Re_x}}\left[\left(\frac{1}{(1-\varphi)^{2.5}} + \frac{\alpha(7n-1)}{2[(1-\varphi)\rho_f + \varphi\rho_s]}\right)f''(0) - \frac{\alpha S(n+1)}{2[(1-\varphi)\rho_f + \varphi\rho_s]}f'''(0)\right], \tag{20}$$

$$Nu = -\frac{(k_s + 2k_f) - 2\varphi(k_f - k_s)}{(k_s + 2k_f) + \varphi(k_f - k_s)}\sqrt{\frac{n+1}{2}Re_x}\,\theta'(0), \tag{21}$$

$$Sh = -\sqrt{\frac{(n+1)}{2}Re}\,\phi'(0), \tag{22}$$

where $Re_x = \frac{bx^{n+1}}{\upsilon_f}$ is the local Reynolds number.

4. Computational Approach

The coupled nonlinear ordinary differential equations governing the flow are reduced to a system of first order ordinary differential equations by letting;

$$f = x_1, f' = x_2, \ f'' = x_3, \ f''' = x_4, \ \theta = x_5, \ \theta' = x_6, \ \theta'' = x_7, \ \phi = x_8, \ \phi' = x_9, \ \phi'' = x_{10}. \tag{24}$$

Substituting equations (24) into equations (13)-(17) yields the required first order system of differential equations as;

$f'(\eta) = x_1' = x_2,$

$f''(\eta) = x_2' = x_3,$

$$f''''(\eta) = x_4' = \frac{2}{(n+1)x_1}\left(\begin{array}{l} (3n-1)x_2x_4 - \frac{(3n-1)}{2}x_3^2 - \\ \frac{(1-\varphi)\rho_f + \varphi\rho_s}{\rho_f\alpha_v}\left[\begin{array}{l} \frac{\rho_f}{(1-\varphi)^{2.5}\left((1-\varphi)\rho_f + \varphi\rho_s\right)}x_4 - \\ \frac{2}{n+1}\frac{\rho_f K^*}{(1-\varphi)^{2.5}\left((1-\varphi)\rho_f + \varphi\rho_s\right)}x_2 - \\ \frac{2n}{n+1}x_2^2 + x_1x_3 \end{array}\right] \end{array}\right)$$

$$\theta'(\eta) = x_5' = x_6,$$

$$\theta''(\eta) = x_6' = x_7 = -\frac{(k_s + 2k_f) + \varphi(k_f - k_s)}{(k_s + 2k_f) - 2\varphi(k_f - k_s)}\left[\begin{array}{l} \frac{(1-\varphi)(\rho c_p)_f + \varphi(\rho c_p)_s}{(\rho c_p)_f}\Pr x_1x_6 + \frac{Br}{(1-\varphi)^{2.5}}x_3^2 + \\ Br\alpha_v\left[\frac{(3n-1)}{2}x_2x_3^2 - \frac{(n+1)}{2}x_1x_3x_4\right] + \\ \frac{(1-\varphi)(\rho c_p)_f + \varphi(\rho c_p)_s}{(\rho c_p)_f}\Pr D_o x_{10} \end{array}\right]$$

$$\varphi' = x_8' = x_9$$

$$\phi''(\eta) = x_9' = x_{10} = \frac{2}{n+1}Sc\beta x_8 - Scx_1x_9 - ScS_o x_7\,. \tag{25}$$

Subject to the boundary conditions;

$$x_2 = 1,\ x_1 = S,\ x_6 = -Bi(1-g),\ x_8 = 1,\ x_2 = e,\ x_3 = f,\ x_5 = g,\ x_8 = h. \tag{26}$$

The unknowns; e, f, g and h were approximated using the Shooting technique and the resulting initial value problem solved using the fourth order Runge Kutta integration scheme. Numerical computations are done using MAPLE 18 software package.

5. Results and Discussions

The entrenched thermophysical parameters considered in this study are the viscoelastic parameter (α_v), nonlinear stretching parameter (n), Dufour number (D_o), Soret number (S_o), Schmidt number (Sc), chemical reaction rate parameter (β), solid volume fraction of nanoparticles (φ), permeability parameter (K^*), Prandtl number (Pr), Biot number (Bi), Brinkman number (Br) and suction parameter (S). The thermophysical properties of oil and nanoparticles are presented in Table 1.

Table 1: Thermophysical properties of oil and nanoparticles

Physical property	C_p [J/kgK]	ρ [Kg/m^3]	k [W/mK]
Oil	1670	920	0.138
CuO	540	6510	18
Al_2O_3	765	3970	40

5.1. Numerical Results

The results of the present model for the local Nusselt number denoted by $(-\theta'(0))$ were compared with the work of Cortell [29] for varying values of the Prandtl number (Pr) and nonlinear stretching parameter (n) and for $q = G_T = Br = S = Bi = \varphi = \alpha = \sigma = K^* = 0$ with convective boundary condition. The perfect agreement with the results of Cortell [27] up to four decimal places authenticates the present numerical scheme. The comparison is presented in Table 2.

Table 2: Computations showing comparison with Cortell [29] for
$q = G_T = Br = S = Bi = \varphi = \alpha = \sigma = K^* = 0$

		Cortell [29]	Present Work
Pr	**N**	$-\theta'(0)$	$-\theta'(0)$
1.0	**0.2**	**0.610262**	**0.610216**
	0.5	**0.595277**	**0.595224**
	1.5	**0.574537**	**0.574771**
5.0	**0.2**	**1.607175**	**1.607784**
	0.5	**1.586744**	**1.586779**
	1.5	**1.557463**	**1.557691**

The influence of the various thermophysical parameters on the skin friction coefficient $(-f''(\theta))$, Nusselt number $(-\theta'(0))$ and Sherwood number $(-\phi'(0))$ for both Al_2O_3-oil based nanofluid and CuO-oil based nanofluid are presented in Table 3. It is evident in the Table that increasing the viscoelastic parameter decreased both the skin friction coefficient and Nusselt number but increased the Sherwood number. This can be attributed to the fact that a hike in the viscoelastic parameter corresponds to decaying shearing stresses which impede the rate of heat transfer at the surface of the plate but accelerated the rate of mass transfer of the nanoparticles at surface of the plate. CuO-oil based nanofluid was seen to exhibit higher enhancement in the Sherwood number and reduction in the skin friction coefficient while Al_2O_3-oil based nanofluid recorded higher reduction in the Nusselt number. An increase in the solid volume fraction was seen to increase the skin friction coefficient but decreased both the Nusselt and Sherwood numbers. The skin friction coefficient was noted to show higher appreciation with CuO-oil based nanofluid while both the Nusselt and Sherwood numbers showed tremendous reduction with Al_2O_3-oil based nanofluid. A hike in both the permeability and suction parameters increased both the Nusselt and Sherwood numbers but decreased the skin friction coefficient. An increase in these parameters boosts both the rates of heat and mass transfer at the surface of the plate. The Nusselt and Sherwood numbers were noted to be high for CuO-oil based nanofluid while the skin friction coefficient was lower for the same nanofluid. But increasing the nonlinear stretching parameter degraded the skin friction coefficient, Nusselt number and Sherwood number. Al_2O_3-oil based nanofluid recorded lower Nusselt number while CuO-oil based nanofluid also exhibited lower skin friction coefficient and Sherwood number. The Dufour number is noted not to influence the skin friction coefficient but it increased the Sherwood number and decayed the Nusselt number. This is because an increase in the Dufour number corresponds to higher molecular diffusion of the nanoparticles which accelerates the rate of mass transfer of the nanoparticles from the surface but it retards the rate of heat transfer at the surface of the plate. The Nusselt and Sherwood numbers were high for CuO-oil based nanofluid while Al_2O_3-oil based nanofluid recorded higher value for the skin friction coefficient. Similar trend was noted with the Schmidt number and chemical reaction rate parameter as an increase in these parameters enhance the momentum diffusivity of the nanoparticles but the dominance of the diffusion rate boosts the rate of mass transfer of these nanoparticles from the surface of the plate. A simultaneous rise in both Prandtl and Biot numbers did not affect the skin friction coefficient but it decreased the Nusselt number with Al_2O_3-oil based nanofluid recording the higher depletion while it appreciated the Sherwood number with CuO-oil based nanofluid indicating better enhancement. Higher values of these parameters promote the rate of heat transfer from the surface of the plate due to viscous dissipation and thermal resistance of the nanoparticles. Finally, the Soret number was noted to decrease the magnitudes of both the Nusselt and Sherwood numbers but did influence the skin friction coefficient. Al_2O_3-oil based nanofluid was observed to present higher reduction in both the Nusselt number and Sherwood numbers. Generally, increasing the Soret number increases the temperature of the mixture but clustering of the nanoparticles decrease the temperature which slows the rates of heat and mass transfer at the surface of the plate.

Table 3: Computation showing $(-f''(0))$, $(-\theta'(0))$ and $(-\phi'(0))$ for different parameter values

α_v	φ	Pr	K^*	Br	n	S	D_o	S_o	Sc	β	Bi	$-f''(0)$ **Al_2O_3 CuO**	$-\theta'(0)$ **Al_2O_3 CuO**	$-\phi'(0)$ **Al_2O_3 CuO**
1	0.10	100	0.1	1	2	0.1	0.1	0.1	0.1	0.1	0.1	1.045739	0.091857	0.528302
												0.949159	0.092632	0.528795
2												1.000449	0.088758	0.529085
												0.965412	0.089368	0.529252
	0.15											1.098098	0.091346	0.527924
												0.933214	0.092630	0.528750
	0.20											1.222751	0.090197	0.527184
												0.955278	0.092296	0.528462
		120										1.045739	0.092909	0.528239
												0.949159	0.093573	0.528738
		140										1.045739	0.093682	0.528193
												0.949159	0.094263	0.528697
			1.0									0.884628	0.092829	0.529093
												0.787568	0.093519	0.529620
			2.0									0.709082	0.093754	0.530000
												0.611930	0.094347	0.530562
				3								1.045739	0.079221	0.529060
												0.949159	0.081509	0.529462
				5								1.045739	0.066586	0.529819
												0.949159	0.070385	0.530129
					4							0.997038	0.088436	0.527326

							0.956688	0.089123	0.527525
6							0.993214	0.084667	0.526923
							0.967449	0.085405	0.527034
	0.2						0.988039	0.093801	0.533758
							0.897827	0.094343	0.534240
	0.3						0.948631	0.094877	0.539177
							0.862215	0.095297	0.539654
		0.3					1.045739	0.089597	0.528437
							0.949159	0.090390	0.528929
		0.5					1.045739	0.087292	0.528576
							0.949159	0.088106	0.529066
			0.4				1.045739	0.091825	0.526779
							0.949159	0.092627	0.527125
			0.7				1.045739	0.091771	0.525280
							0.949159	0.092606	0.525467
				0.2			1.045739	0.090738	0.557144
							0.949159	0.091523	0.558139
				0.3			1.045739	0.089616	0.586493
							0.949159	0.090410	0.587996
					1.0		1.045739	0.090476	0.567222
							0.949159	0.091267	0.567693
					2.0		1.045739	0.088988	0.609105
							0.949159	0.089795	0.609555
						1.0	1.045739	0.863151	0.520874
							0.949159	0.871844	0.521283
						3.0	1.045739	2.283341	0.507196
							0.949159	2.313208	0.507387

5.2. Graphical Results

Effects of Parameter Variation on Velocity Profiles

The influence of the various thermophysical parameters on the velocity profiles for both CuO-oil based and Al_2O_3-oil based nanofluid are presented in Figures 2-6. The effect of viscoelastic parameter on the velocity profiles is depicted in Figure 2. It is seen in the Figure that increasing the viscoelastic parameter accelerates the velocity of the oil-based nanofluid. This is because an increase in the viscoelastic parameter weakens the internal resistance the nanofluid offers to deformation and as a result increases the velocity of the nanofluid within the boundary layer which intend thickens the momentum boundary layer. CuO-oil based nanofluid is seen to exhibit higher enhancement in the momentum boundary layer thickness. It is also observed in Figures 3 and 4 that increasing the suction and permeability parameters increase both the velocity of the nanofluid and momentum boundary layer thickness. While it is noted in Figures 5 and 6 that increasing the solid volume fraction of nanoparticles and nonlinear stretching parameter deplete the momentum boundary layer thickness due to the retardation of the rate of heat transfer at the surface of the plate. Al_2O_3-oil based nanofluid recorded higher retardation in its momentum boundary layer thickness.

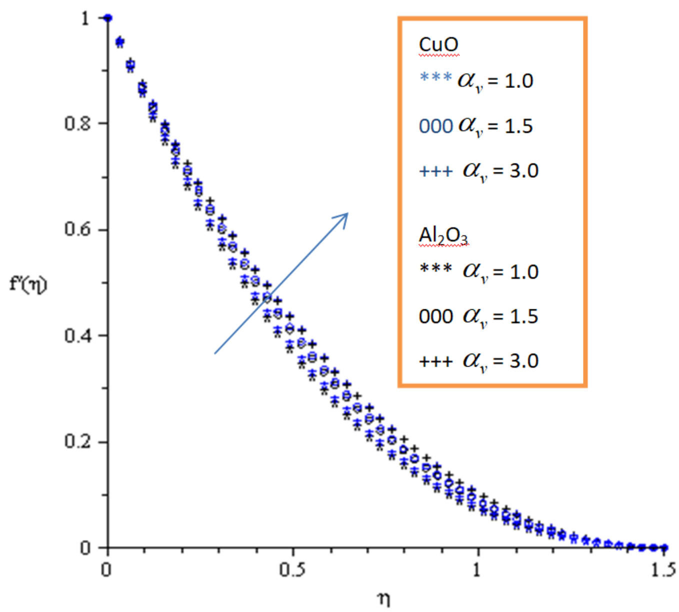

Figure 2: Velocity profile for varying values of viscoelastic parameter for $\Pr = 100$, $S = 0.1$, $Sc = 0.1$, $K^* = 0.1$, $n = 2$, $S_o = 0.1$, $\beta = 0.1$, $Bi = 0{,}1$, $D_0 = 1$, $\varphi = 0.1$ and $Br = 1$.

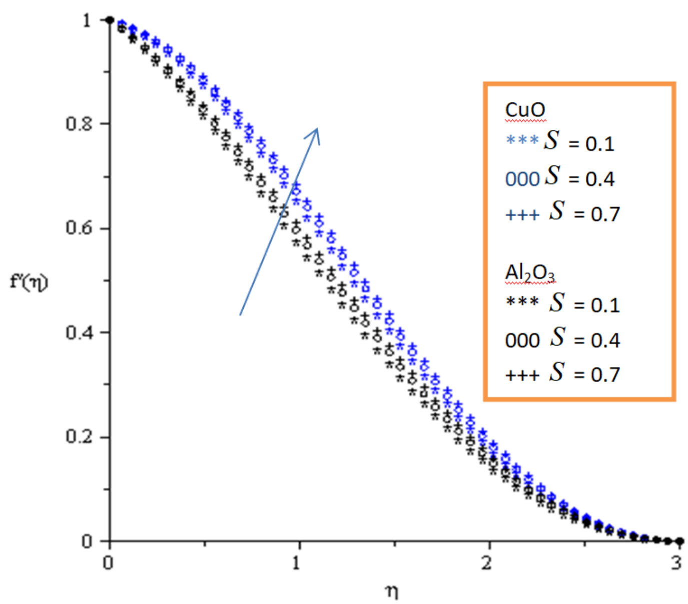

Figure 3: Velocity profile for varying values of suction parameter for $\Pr = 100$, $\alpha_v = 1$, $Sc = 0.1$, $K^* = 0.1$, $n = 2$, $S_o = 0.1$, $\beta = 0.1$, $Bi = 0{,}1$, $D_0 = 1$, $\varphi = 0.1$ and $Br = 1$.

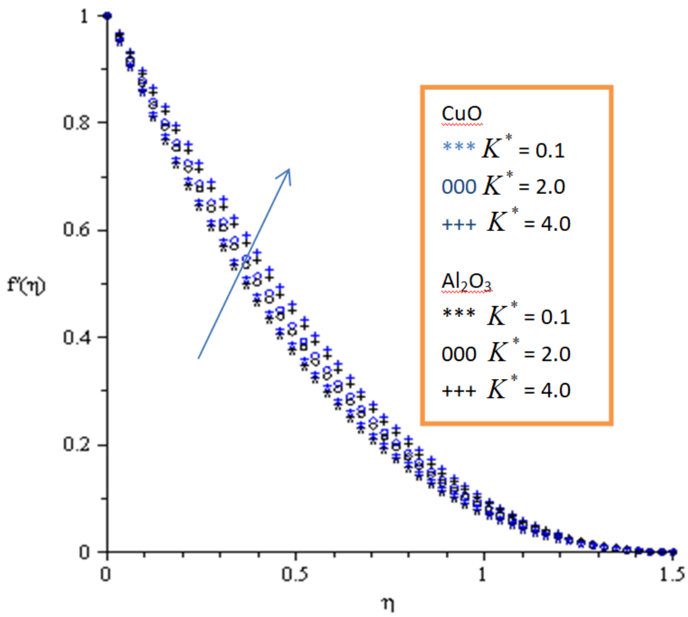

Figure 4: Velocity profile for varying values of permeability parameter for $\Pr = 100$, $\alpha_v = 1$, $Sc = 0.1$, $S = 0.1$, $n = 2$, $S_o = 0.1$, $\beta = 0.1$, $Bi = 0{,}1$, $D_0 = 1$, $\varphi = 0.1$ and $Br = 1$.

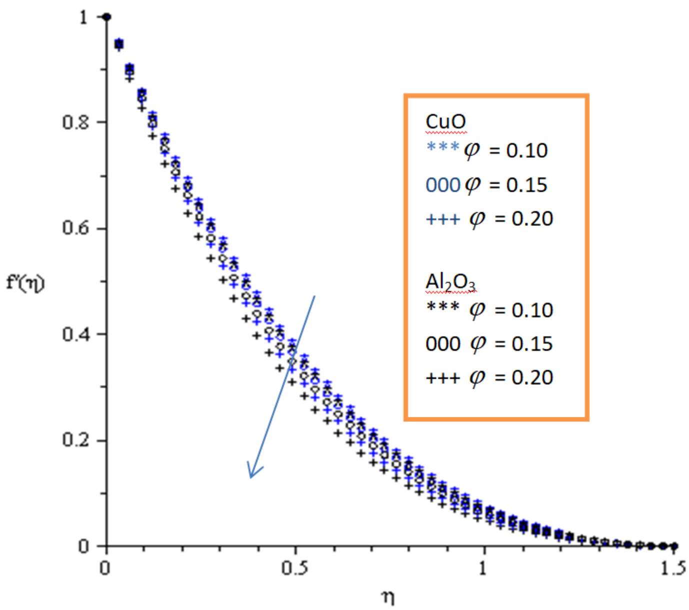

Figure 5: Velocity profile for varying values of solid volume fraction of nanoparticles for $\Pr = 100$, $\alpha_v = 1$, $Sc = 0.1$, $S = 0.1$, $n = 2$, $S_o = 0.1$, $\beta = 0.1$, $Bi = 0{,}1$, $D_0 = 1$, $K^* = 0.1$ and $Br = 1$.

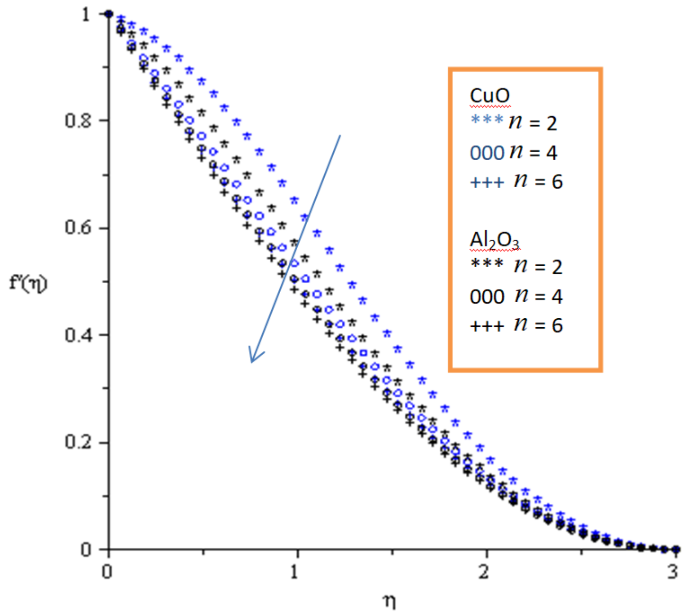

Figure 6: Velocity profile for varying values of nonlinear stretching parameter for $\Pr = 100$, $\alpha_v = 1$, $Sc = 0.1$, $S = 0.1$, $\varphi = 0.1$, $S_o = 0.1$, $\beta = 0.1$, $Bi = 0{,}1$, $D_0 = 1$, $K^* = 0.1$ and $Br = 1$.

Effects of Parameter Variation on Temperature Profiles

Figures 7-18 present the temperature profiles for both CuO-oil based and Al_2O_3-oil based nanofluids for varying values of the thermophysical parameters. The influence of the viscoelastic parameter on the temperature profile is portrayed in Figure 7. It is noted that increasing the viscoelastic parameter increases both the temperature of the nanofluid and thermal boundary layer thickness. Al_2O_3-oil based nanofluid showed higher enhancement in the thermal boundary layer thickness. Figures 8-13 also show that increasing the Brinkman number, chemical reaction rate, Biot number, Dufour number, solid volume fraction of nanoparticles, nonlinear stretching parameter and Schmidt number enhance both the temperature of the nanofluid and thermal boundary layer thickness. This is as a result of excessive heating due to viscous dissipation, internal thermal resistance of the nanoparticles, Brownian motion of the nanoparticles and enhanced molecular diffusion. But it is observed in Figure 14 that increasing the Prandtl number deteriorates both the temperature of the nanofluid and thermal boundary layer thickness. This can be attributed to the depletion of the heat transfer rate at the surface of the plate due to the degradation of the thermal diffusivity of the nanofluid. CuO-oil based nanofluid exhibited higher depletion in its thermal boundary layer thickness. Similar trends were noted in Figures 15-18 as the intensities of the Prandtl number, permeability parameter, suction parameter and Soret number were increased. These parameters decrease the thermal diffusivity of the nanofluid.

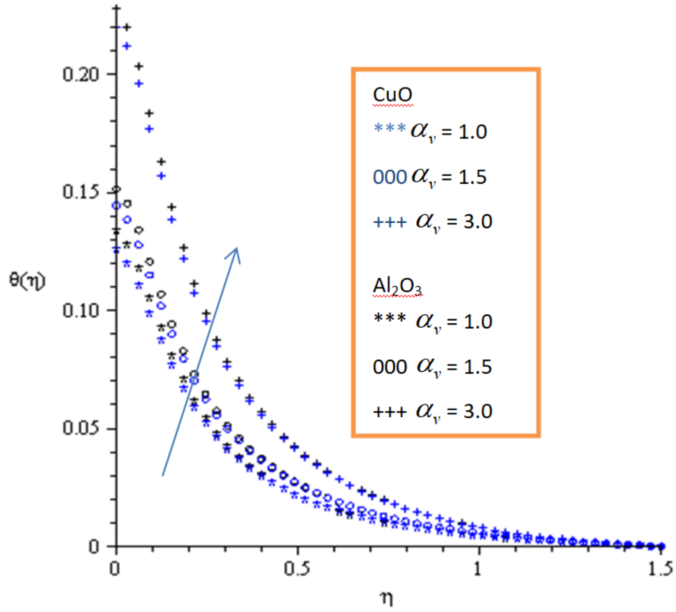

Figure 7: Temperature profile for varying values of viscoelastic parameter for $\Pr = 100$, $S = 0.1$, $Sc = 0.1$, $K^* = 0.1$, $n = 2$, $S_o = 0.1$, $\beta = 0.1$, $Bi = 0{,}1$, $D_0 = 1$, $\varphi = 0.1$ and $Br = 1$.

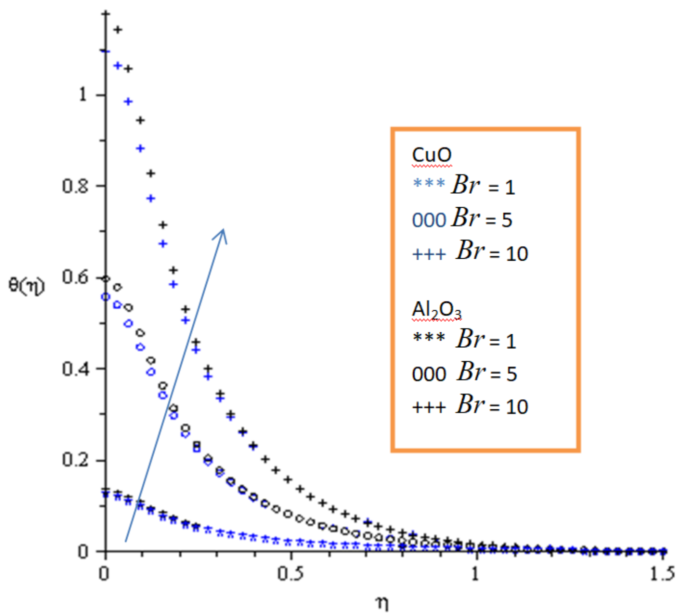

Figure 8: Temperature profile for varying values of Brinkman number for $\Pr = 100$, $S = 0.1$, $Sc = 0.1$, $K^* = 0.1$, $n = 2$, $S_o = 0.1$, $\beta = 0.1$, $Bi = 0{,}1$, $D_0 = 1$, $\varphi = 0.1$ and $\alpha_v = 1$.

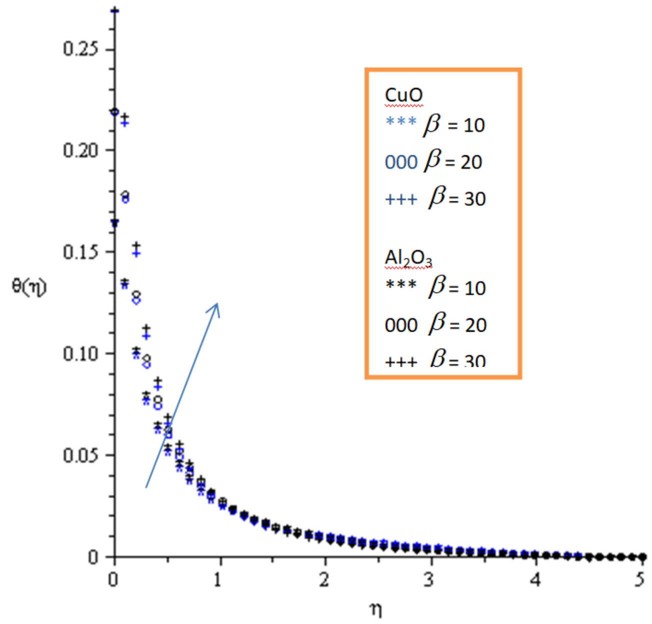

Figure 9: Temperature profile for varying values of chemical reaction rate parameter for $\Pr = 100$, $S = 0.1$, $Sc = 0.1$, $K^* = 0.1$, $n = 4$, $S_o = 0.1$, $Br = 1$, $Bi = 0{,}1$, $D_0 = 1$, $\varphi = 0.1$ and $\alpha_v = 1$.

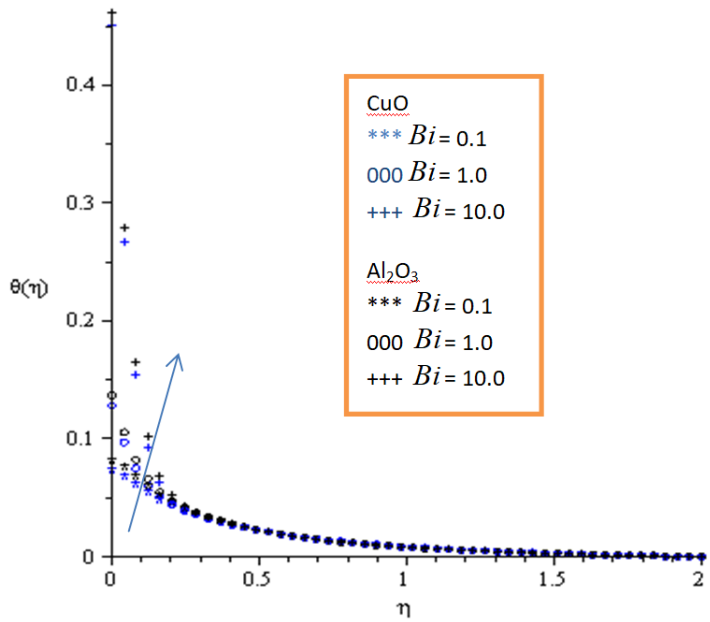

Figure 10: Temperature profile for varying values of Biot number for $\Pr = 100$, $S = 0.1$, $Sc = 0.1$, $K^* = 0.1$, $n = 2$, $S_o = 0.1$, $Br = 1$, $\beta = 0.1$, $D_0 = 1$, $\varphi = 0.1$ and $\alpha_v = 1$.

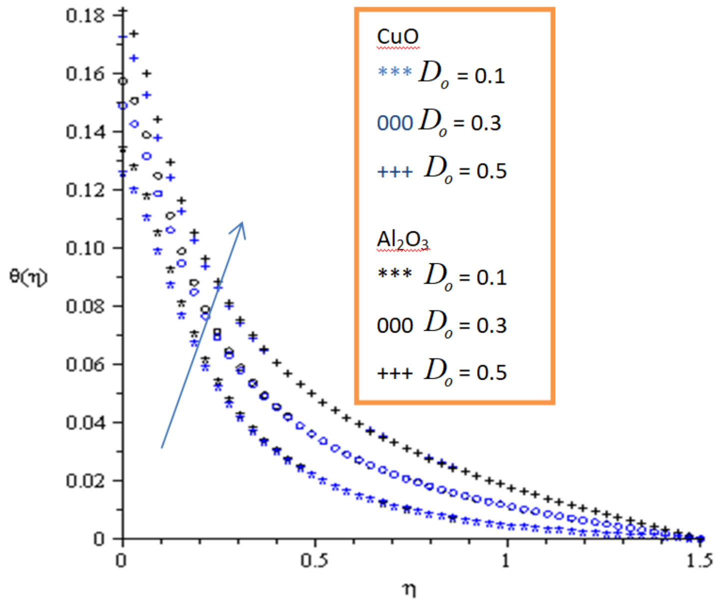

Figure 11: Temperature Profile for varying values of Dufour number for $\Pr = 100$, $S = 0.1$, $Sc = 0.1$, $K^* = 0.1$, $n = 2$, $S_o = 0.1$, $Br = 1$, $\beta = 0.1$, $Bi = 0.1$, $\varphi = 0.1$ and $\alpha_v = 1$.

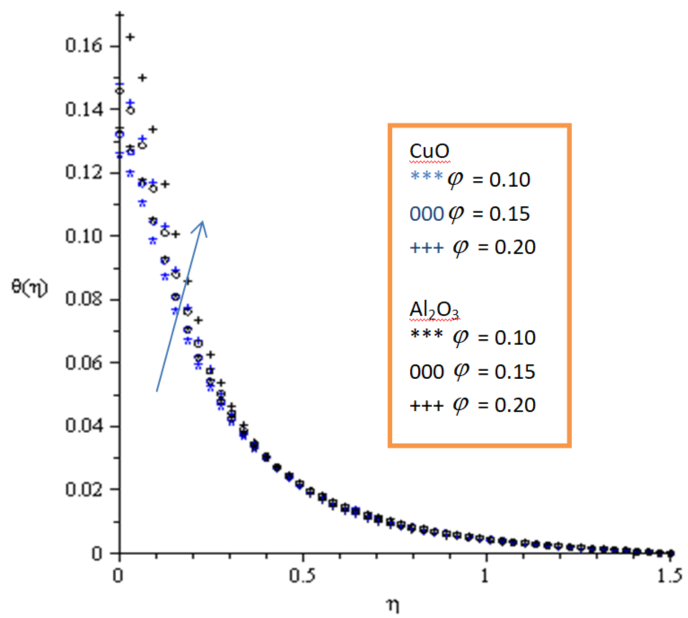

Figure 12: Temperature profile for varying values of solid volume fraction of nanoparticles for $\Pr = 100$, $\alpha_v = 1$, $Sc = 0.1$, $S = 0.1$, $n = 2$, $S_o = 0.1$, $\beta = 0.1$, $Bi = 0.1$, $D_0 = 1$, $K^* = 0.1$ and $Br = 1$.

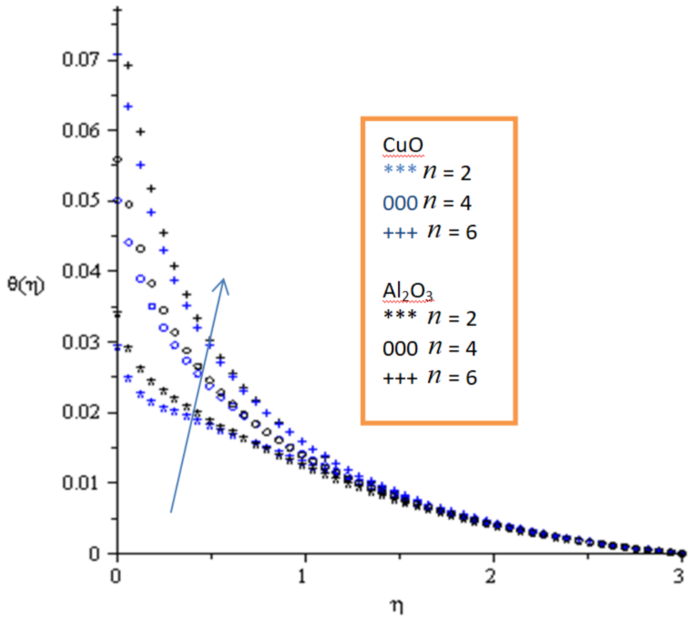

Figure 13: Temperature profile for varying values of nonlinear stretching parameter for $\Pr = 100, \alpha_v = 1,$ $Sc = 0.1,\ S = 0.1,\ \varphi = 0.1,\ S_o = 0.1,\ \beta = 0.1,\ Bi = 0.1,\ D_0 = 1,\ K^* = 0.1$ and $Br = 1$.

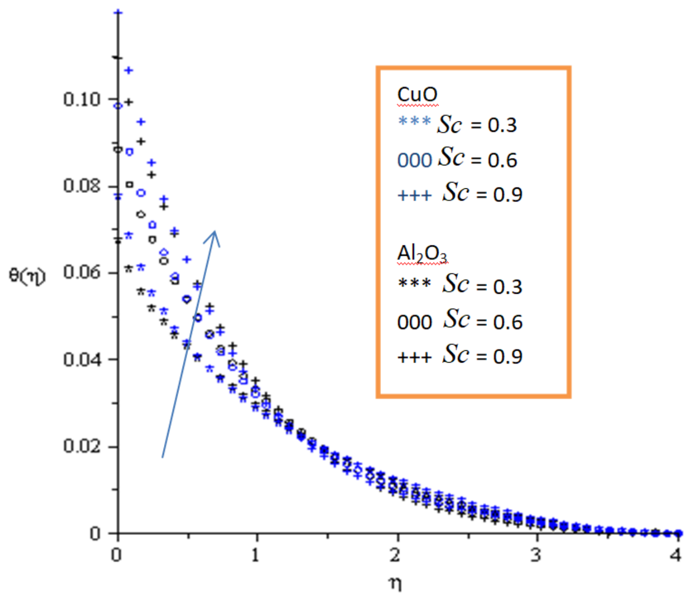

Figure 14: Temperature profile for varying values of Schmidt number for $\Pr = 100, \alpha_v = 1,\ n = 2,\ S = 0.1,$ $\varphi = 0.1,\ S_o = 0.1,\ \beta = 0.1,\ Bi = 0.1,\ D_0 = 1,\ K^* = 0.1$ and $Br = 1$.

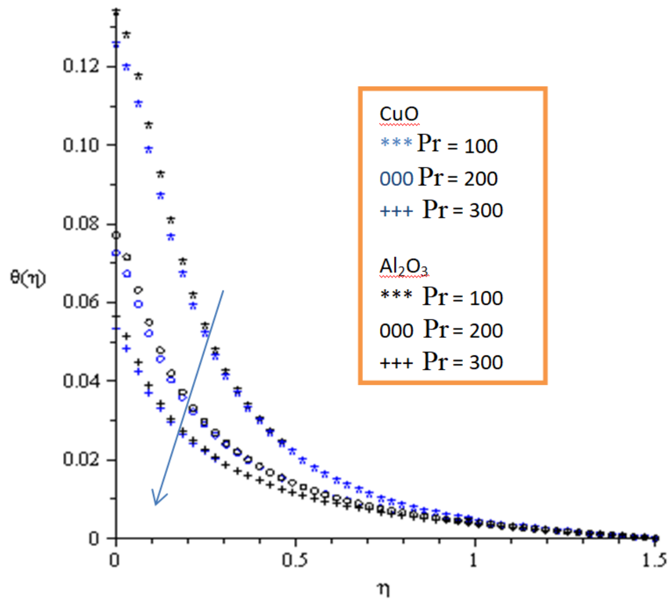

Figure 15: Temperature profile for varying values of Prandtl number for $Sc = 0.1$, $\alpha_v = 1$, $n = 2$, $S = 0.1$, $\varphi = 0.1$, $S_o = 0.1$, $\beta = 0.1$, $Bi = 0.1$, $D_0 = 1$, $K^* = 0.1$ and $Br = 1$.

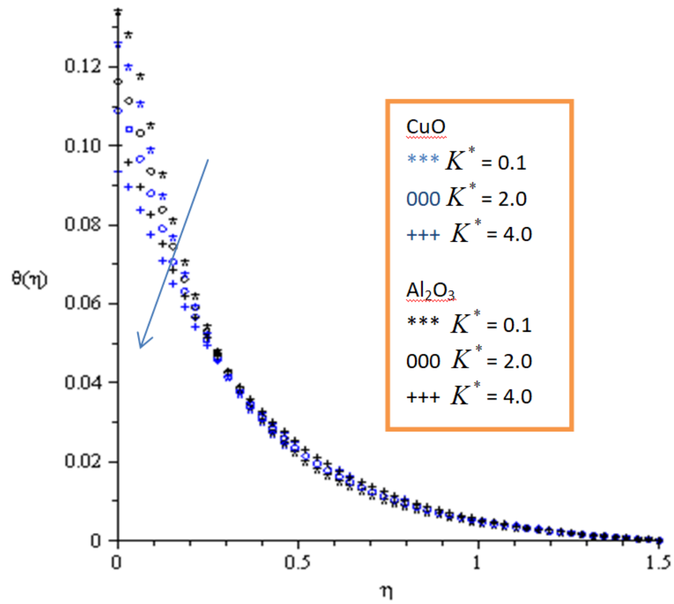

Figure 16: Temperature profile for varying values of permeability parameter for $\Pr = 100$, $\alpha_v = 1$, $Sc = 0.1$, $S = 0.1$, $n = 2$, $S_o = 0.1$, $\beta = 0.1$, $Bi = 0{,}1$, $D_0 = 1$, $\varphi = 0.1$ and $Br = 1$.

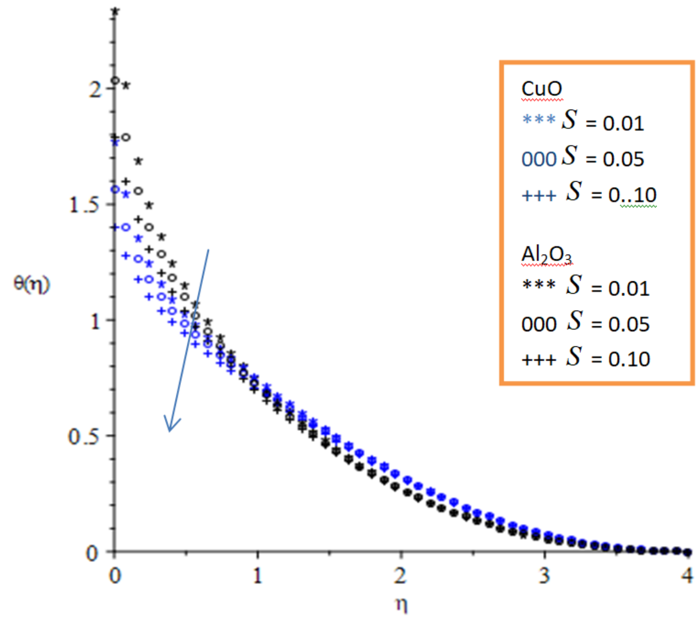

Figure 17: Temperature Profile for varying values of suction parameter for $\Pr = 100$, $\alpha_v = 1$, $Sc = 0.1$, $K^* = 0.1$, $n = 4$, $S_o = 0.1$, $\beta = 0.1$, $Bi = 1$, $D_0 = 1$, $\varphi = 0.1$ and $Br = 100$.

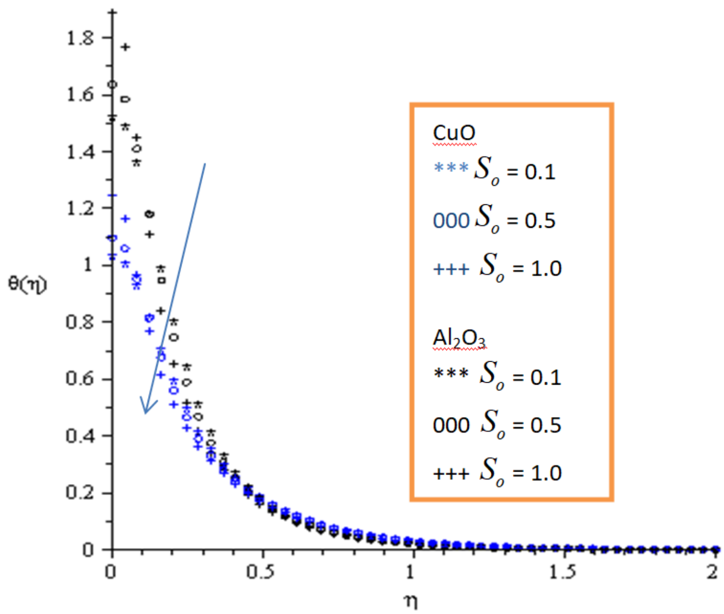

Figure 18: Temperature profile for varying values of Soret number for $\Pr = 100$, $\alpha_v = 1$, $Sc = 0.1$, $K^* = 0.1$, $n = 2$, $S = 0.01$, $\beta = 0.1$, $Bi = 0{,}1$, $D_0 = 1$, $\varphi = 0.2$ and $Br = 1$.

Effects of Parameter Variation on Concentration Profiles

Figures 19-22 present the concentration profiles for both CuO-oil based and Al_2O_3-oil based nanofluids for varying values of the thermophysical parameters. The concentration of the nanofluid is peak at the surface of the plate and decreases gradually to the free stream zero value far away from the plate. The effect of Soret number on the concentration profile is illustrated in Figure 19. It is noted in the Figure that increasing the Soret number increases the concentration of the nanoparticles and the solutal boundary layer thickness. Physically, increasing the Soret number increases the thermal diffusivity of the nanofluid. Al_2O_3-oil based nanofluid recorded higher enhancement in the solutal boundary layer thickness. However, it is seen in Figure 20, that increasing the Schmidt number decreases both the concentration of the nanofluid and solutal boundary layer thickness. Physically, a hike in the Schmidt number corresponds to a decrease in the molecular diffusion rate. CuO-oil based nanofluid showed higher depletion in the solutal boundary layer thickness. Figures 21 and 22 also show that increasing the suction and chemical reaction rate parameters deplete both the concentration of the nanofluid and solutal boundary layer thickness due to a hike in the concentration gradient.

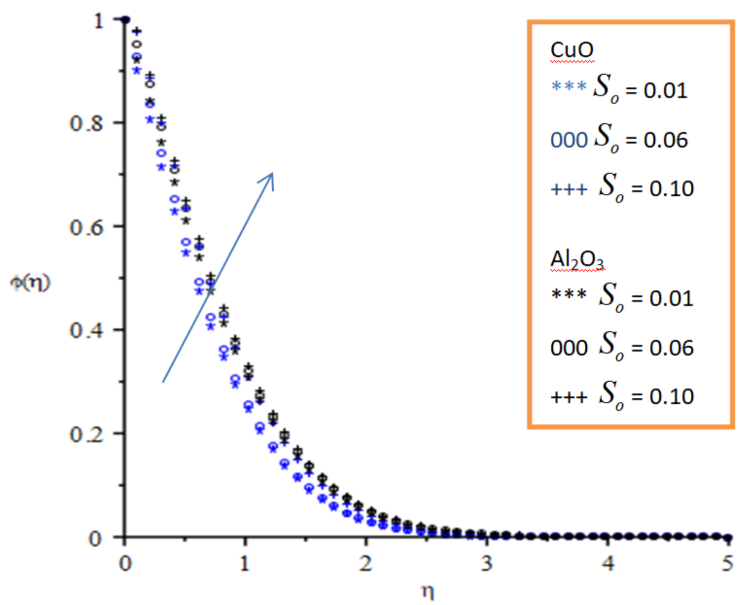

Figure 19: Concentration profile for varying values of Soret number for $\Pr = 100$, $\alpha_v = 1$, $Sc = 0.1$, $K^* = 0.1$, $n = 2$, $S = 0.01$, $\beta = 0.1$, $Bi = 100$, $D_0 = 1$, $\varphi = 0.2$ and $Br = 10$.

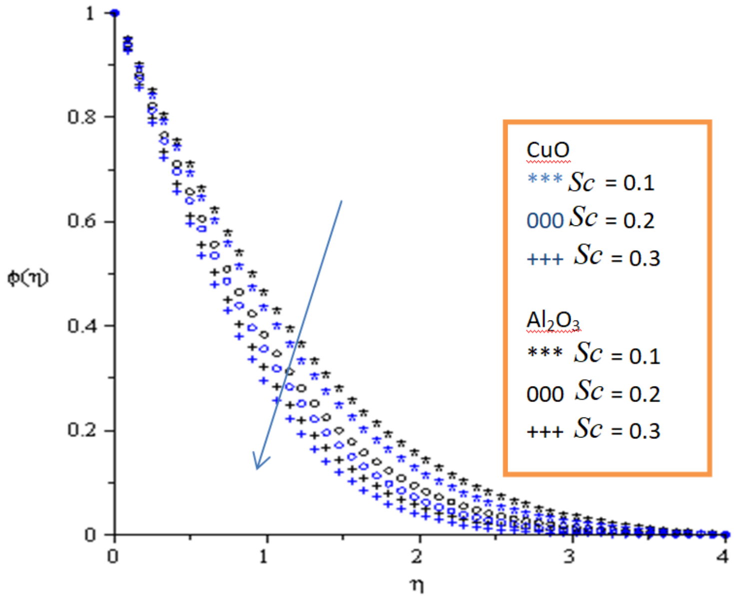

Figure 20: Concentration Profile for varying values of Schmidt number for $\Pr = 100$, $\alpha_v = 1$, $n = 2$, $S = 0.1$, $\varphi = 0.1$, $S_o = 0.1$, $\beta = 0.1$, $Bi = 0.1$, $D_0 = 1$, $K^* = 0.1$ and $Br = 1$.

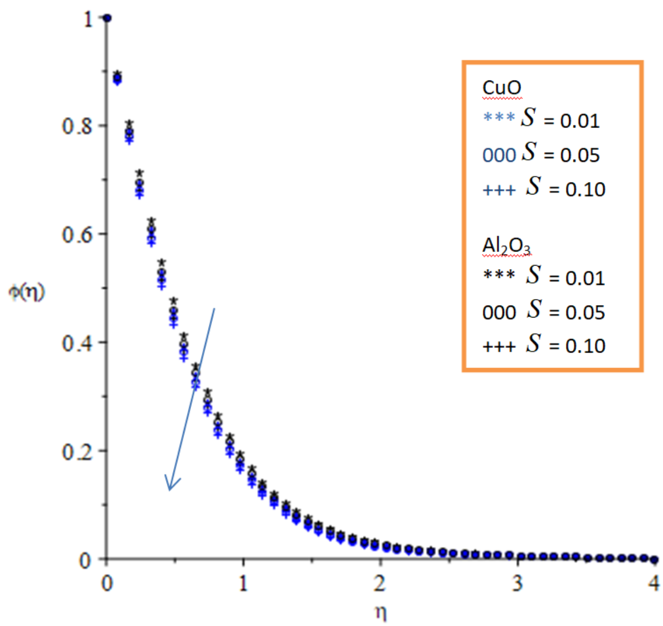

Figure 21: Concentration profile for varying values of suction parameter for $\Pr = 100$, $\alpha_v = 1$, $Sc = 0.1$, $K^* = 0.1$, $n = 4$, $S_o = 0.1$, $\beta = 0.1$, $Bi = 1$, $D_0 = 1$, $\varphi = 0.1$ and $Br = 100$.

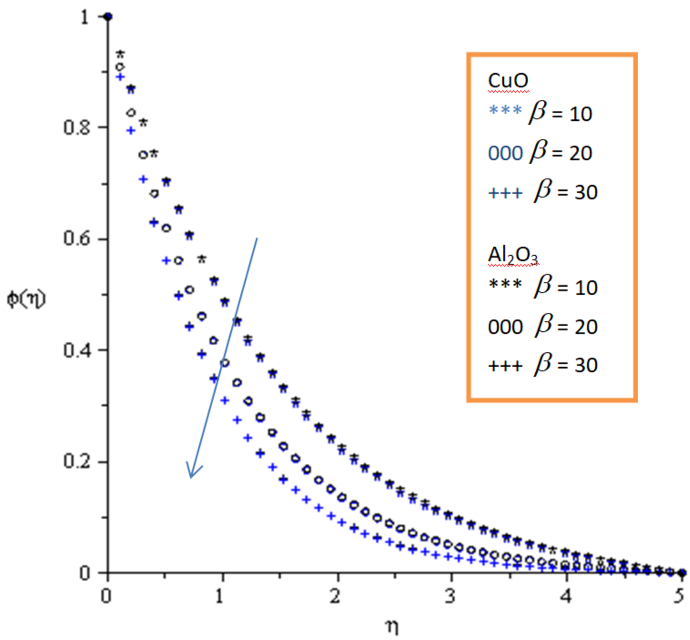

Figure 22: Concentration profile for varying values of chemical reaction rate parameter for $\Pr = 100$, $S = 0.1$, $Sc = 0.1$, $K^* = 0.1$, $n = 4$, $S_o = 0.1$, $Br = 1$, $Bi = 0{,}1$, $D_0 = 1$, $\varphi = 0.1$ and $\alpha_v = 1$.

6. Conclusions

Chemical reaction and Cross diffusion effects on heat and mass transport characteristics of viscoelastic flow of Al_2O_3 and CuO oil-based nanofluids past a porous nonlinear stretching surface have been studied. The fourth order Runge-Kutta algorithm with a shooting method was used to solve the coupled nonlinear ordinary differential equations governing the flow problem. The following conclusions can be drawn from the study.

i. Both Al_2O_3 and CuO oil-based nanofluids show similar rates of heat and mass transfer with the Soret number. They both degraded the Nusselt and Sherwood numbers under the same Soret effect. Under similar conditions, Al_2O_3-oil based nanofluid gave lower drag force.

ii. CuO-oil based nanofluid was noted to exhibit superiority in terms of heat and mass transfer potential over Al_2O_3-oil based nanofluid with the same Dufour effect.

References

[1] Awad, F. G., Sibanda, P., & Khidir, A. (2013). Thermo-diffusion effects on magneto-nanofluid flow over a stretching sheet. *Boundary Value Problems*, *136*(1), 1-13. https://doi.org/10.1186/1687-2770-2013-136

[2] Hayat, T., Rafiq, M., & Ahmad, B. (2016). Soret and Dufour effects on MHD peristaltic flow of Jeffrey fluid in a rotating system with porous medium. *PLoS ONE*, *11*(1), e0145525. https://doi.org/10.1371/journal.pone.0145525

[3] Kasmani, R. Md., Sivasankaran, S., Bhuvaneswari, M., & Hussein, A. K. (2017). Analytical and numerical study on convection of nanofluid past a moving wedge with Soret and Dufour effects. *International Journal of Numerical Methods for Heat and Fluid Flow*, *27*(10), 2333-2354. https://doi.org/10.1108/HFF-07-2016-0277

[4] Salleh, N. H. M., Amirsom, N. A., Abdul-Latiff, N. A., Basir, M. F. M., & Ismail, A. I. Md. (2018). Dufour and Soret effects on magnetohydrodynamic boundary layer slip flow in nanofluids with microorganisms over a heated

stretching sheet with temperature-dependent viscosity. *Menemui Matematik* (*Discovering Mathematics*), *40*(2), 46-63.

[5] Rao, T. R., Kumar, S. S., & Gangadhar, K. (2018). Soret and Dufour effects on magneto-nanofluid flow over a stretching sheet in the presence of thermal radiation and heat generation/absorption. *International Journal of Mathematics Trends and Technology*, *55*(7), 482-497. https://doi.org/10.14445/22315373/IJMTT-V55P563

[6] Najib, N., Bachok, N., Arifin, N. Md., & Ali, F. Md. (2018). Stability analysis of stagnation-point flow in a nanofluid over a stretching/shrinking sheet with second-order slip, Soret and Dufour effects: A revised model. *Applied Sciences*, *8*(4), 642. https://doi.org/10.3390/app8040642

[7] Kumar, B. R., Kumar, M. S., Sandeep, N., & Sivaraj, R. (2018). Cross-diffusion effects on heat and mass transfer micropolar fluid flow past a stretching surface. *Defect and Diffusion Forum*, *388*, 265-280. https://doi.org/10.4028/www.scientific.net/DDF.388.265

[8] Sharma, R., Hussain, S. M., & Mishra, G. (2018). Soret and Dufour effects on viscoelastic radiative and heat-absorbing nanofluid driven by a stretched sheet with inclined magnetic field. *Defect and Diffusion Forum*, *388*, 223-245. https://doi.org/10.4028/www.scientific.net/DDF.388.223

[9] Kandasamy, R., Dharmalingam, R., & Prabhu, K. K. S. (2018). Thermal and solutal stratification on MHD nanofluid flow over a porous vertical plate. *Alexandria Engineering Journal*, *57*, 121-130. https://doi.org/10.1016/j.aej.2016.02.029

[10] Lakshmi, K. B., Kumar, K. A., Reddy, J. V. R., & Sugunamma, V. (2019). Influence of nonlinear radiation and cross-diffusion on MHD flow of Casson and Walters-B nanofluids past a variable thickness sheet. *Journal of Nanofluids*, *8*, 1-11. https://doi.org/10.1166/jon.2019.1564

[11] Bhuvaneswari, M., Eswaramoorthi, S., Sivasankaran, S., & Hussein, A. K. (2019). Cross-diffusion effects on MHD mixed convection over a stretching surface in a porous medium with chemical reaction and convective condition. *Engineering Transactions*, *67*(1), 3-19.

[12] Aghbari, A., Agha, H. A., Sadaoui, D., & Mouloud, S. (2019). Soret and Dufour effects on non-Darcy natural convection flow of Buongiorno nanofluid over a vertical plate in a porous medium in the presence of viscous dissipation. *Defect and Diffusion Forum*, *392*, 60-72. https://doi.org/10.4028/www.scientific.net/DDF.392.60

[13] Idowu, A. S., & Falodun, B. O. (2019). Soret–Dufour effects on MHD heat and mass transfer of Walter's-B viscoelastic fluid over a semi-infinite vertical plate: Spectral relaxation analysis. *Journal of Taibah University for Science*, *13*(1), 49-62. https://doi.org/10.1080/16583655.2018.1523527

[14] Bhaskar, K., Sharma, K., Gupta, S., & Mehta, R. (2020). MHD fluid flow with cross-diffusion effects through a channel using optimal homotopy analysis method. *Science & Technology Asia*, *25*(1), 19-30.

[15] Baako, M., Etwire, C. J., Aloliga, G., & Seini, Y. I. (2023). Dual stratification effects on mixed convective electro-magnetohydrodynamic flow over a stretching plate with multiple slips and cross diffusion. *Earthline Journal of Mathematical Sciences*, *14*(1), 75-103. https://doi.org/10.34198/ejms.14124.075103

[16] Kumar, R. M., Raju, R. S., Mebarek-Oudina, F., Kumar, M. A., & Narla, V. K. (2024). Cross-diffusion effects on an MHD Williamson nanofluid flow past a nonlinear stretching sheet immersed in a permeable medium. *Frontiers in Heat and Mass Transfer*, *22*(1), 15-34. https://doi.org/10.32604/fhmt.2024.048045

[17] Chitra, M., Jeevitha, S., & Rushi Kumar, B. (2023). Effects of cross diffusion on radiative MHD flow over a rotating cone through porous medium. *Numerical Heat Transfer, Part B: Fundamentals*, 1-19. https://doi.org/10.1080/10407790.2023.2292750

[18] Sahoo, A. C., & Biswal, T. (2015). MHD visco-elastic boundary layer flow past a stretching plate with heat transfer. *International Journal of Engineering Technology, Management and Applied Sciences*, *3*(9), 11-18.

[19] Shit, G. C., Haldar, R., & Ghosh, S. K. (2016). Convective heat transfer and MHD viscoelastic nanofluid flow induced by a stretching sheet. *International Journal of Applied and Computational Mathematics*, *2*, 593-608. https://doi.org/10.1007/s40819-015-0080-4

[20] Etwire, C. J., Seini, I. Y., Rabiu, M., & Makinde, O. D. (2018). Effects of viscoelastic oil-based nanofluids on a porous nonlinear stretching surface with variable heat source/sink. *Defect and Diffusion Forum – Computational Analysis of Heat Transfer in Fluids and Solids*, *387*, 260-272. https://doi.org/10.4028/www.scientific.net/DDF.387.260

[21] Narayana, P. V. S., Tarakaramu, N., Makinde, O. D., Venkateswarlu, B., & Sarojamma, G. (2018). MHD stagnation point flow of viscoelastic nanofluid past a convectively heated stretching surface. *Defect and Diffusion Forum*, *387*, 106-120. https://doi.org/10.4028/www.scientific.net/DDF.387.106

[22] Mahat, R., Rawi, N. A., Kasim, A. R., & Shafie, S. (2018). Mixed convection flow of viscoelastic nanofluid past a horizontal circular cylinder with viscous dissipation. *Sains Malaysiana*, *47*(7), 1617-1623. https://doi.org/10.17576/jsm-2018-4707-33

[23] Hussain, A., Sarwar, L., Akbar, S., Malik, M. Y., & Ghafoor, S. (2019). Model for MHD viscoelastic nanofluid flow with prominence effects of radiation. *Heat Transfer – Asian Research*, *48*, 463-482. https://doi.org/10.1002/htj.21344

[24] Chaich, Z., Saouli, S., & Rezayguia, I. (2019). Thermodynamic analysis of viscoelastic fluid in a porous medium with prescribed wall heat flux over a stretching sheet subjected to a transitive magnetic field. *Thermal Science*, *23*(1), 219-231. https://doi.org/10.2298/TSCI160919028C

[25] Aloliga, G., Seini, I. Y., & Musah, R. (2022). On MHD flow of non-Newtonian viscoelastic fluid over a stretched magnetized surface. *American Journal of Applied Mathematics*, *10*(2), 29-42. https://doi.org/10.11648/j.ajam.20221002.12

[26] Nan, L., Xiaoping, W., Huanying, X., & Haitao, Q. (2024). Numerical study on radiative MHD flow of viscoelastic fluids with distributed-order and variable-order space fractional operators. *Mathematics and Computers in Simulation*, *215*, 291-305. https://doi.org/10.1016/j.matcom.2023.07.021

[27] Maxwell, J. C. (1973). *A treatise on electricity and magnetism*. UK: Clarendon.

[28] Wang, C. Y. (1989). Free convection on a vertical stretching surface, *Journal of Applied Mathematics and Mechanics/Zeitschriftfur AngewandteMathematik und Mechanik*, *69*(11), 418-420. https://doi.org/10.1002/zamm.19890691115

[29] Cortell, R. (2007). Viscous flow and heat transfer over a nonlinear stretching sheet. *Applied Mathematics and Computation*, *184*, 864-873. https://doi.org/10.1016/j.amc.2006.06.077